
This is an electronic reprint of the original article.
This reprint may differ from the original in pagination and typographic detail.

Wang, Zulin; Halli, Petteri; Hannula, Pyry; Liu, Fupeng; Wilson, Benjamin P.; Yliniemi, Kirsi; Lundström, Mari

Recovery of Silver from Dilute Effluents via Electrodeposition and Redox Replacement

Published in:
Journal of the Electrochemical Society

DOI:
[10.1149/2.0031910jes](https://doi.org/10.1149/2.0031910jes)

Published: 22/05/2019

Published under the following license:
CC BY

Please cite the original version:
Wang, Z., Halli, P., Hannula, P., Liu, F., Wilson, B. P., Yliniemi, K., & Lundström, M. (2019). Recovery of Silver from Dilute Effluents via Electrodeposition and Redox Replacement. *Journal of the Electrochemical Society*, 166(8), E266-E274. <https://doi.org/10.1149/2.0031910jes>

This material is protected by copyright and other intellectual property rights, and duplication or sale of all or part of any of the repository collections is not permitted, except that material may be duplicated by you for your research use or educational purposes in electronic or print form. You must obtain permission for any other use. Electronic or print copies may not be offered, whether for sale or otherwise to anyone who is not an authorised user.



Recovery of Silver from Dilute Effluents via Electrodeposition and Redox Replacement

Zulin Wang,¹ Petteri Halli,¹ Pyry Hannula,¹ Fupeng Liu,¹ Benjamin P. Wilson,^{1,*} Kirsi Yliniemi,^{1,2} and Mari Lundström^{1,z}

¹Department of Chemical and Metallurgical Engineering (CMET), Aalto University School of Chemical Engineering, FI-00076 Aalto, Finland

²Department of Chemistry and Materials Science (CMAT), Aalto University School of Chemical Engineering, FI-00076 Aalto, Finland

In this study, the electrodeposition-redox replacement (EDRR) method was studied for the recovery of minor concentrations of silver from dilute solutions. The parameter optimization was carried out with synthetic solutions similar to silver oxide button battery recycling effluents, consisting of sulfuric acid and concentrated base metal (10 g·L⁻¹ H₂SO₄, 60 g/L Zn²⁺) with a minor amount of silver (100 ppm) and a varying amount of Fe³⁺ ions. Results of these experiments were analyzed both electrochemically and by use of SEM-EDS. The role of dissolved Fe³⁺ ions was studied by varying the concentration from 0 to 1000 ppm and the results showed that although the presence of Fe ions decreased silver recovery efficiency, final product purity was found to increase slightly. The EDRR process was also found to be more effective for Ag recovery and has less energy consumption when Fe³⁺ concentrations are relatively low (≤ 100 ppm) when compared with conventional direct current electrowinning. In the final stage, silver was successfully recovered via EDRR, using the optimized conditions, from a real pregnant leaching solution (PLS) obtained from the leaching of silver oxide batteries.

© The Author(s) 2019. Published by ECS. This is an open access article distributed under the terms of the Creative Commons Attribution 4.0 License (CC BY, <http://creativecommons.org/licenses/by/4.0/>), which permits unrestricted reuse of the work in any medium, provided the original work is properly cited. [DOI: 10.1149/2.0031910jes]



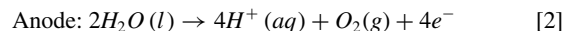
Manuscript submitted December 3, 2018; revised manuscript received March 11, 2019. Published May 22, 2019.

Silver and its compounds are widely used in a diverse range of industries including photography, electronics, medical, chemical and jewelry applications. Generally, silver is obtained as a by-product from base metal production such as zinc,¹ copper,² nickel³ and antimony.⁴ However, the global demand for silver has increased steadily in recent years due to more widespread industrialization and the greater demand for consumer electronics. It has actually been suggested that silver production will reach its peak in 2030 and the future silver supply will be soon at risk (2075) due its rapid consumption and limited availability.⁵ Consequently, this increased demand for silver and the depletion of high grade raw materials has led to the investigation of alternative methods to recover silver from a wide range of secondary raw materials like used PCBs (printed circuit boards),⁶ catalysts⁷ and photographic process wastes⁸. In particular, silver recovery from silver oxide button cells has been studied due to the considerable quantities of the waste material and the high silver content present in them.⁹⁻¹⁴

Silver oxide buttons batteries are widely used in small portable electronic such as toys, watches, digital calculators, hearing aids, etc. due to their high capacity per unit mass and long service life.¹⁵ The cathode of these button batteries typically comprises of silver oxide (Ag₂O) powders, while activated zinc functions as the anode material. Within the battery structure these electrodes are separated by a semi-permeable ion exchange membrane and assembled in a stainless steel case. Worldwide, billions of primary batteries are produced every year, although currently only a very small percentage of consumer disposable batteries are recycled.¹⁴ Therefore, the ability to recover valuable materials from button cells is of considerable interest for both an environmental toxicity and economic point-of-view.

Recycling of waste button batteries generally involves three steps: (i) pretreatment of the cells by crushing, drying, grinding and sieving; (ii) leaching of the valuable metals by nitric acid or bio-leaching agent; (iii) recovery of the valuable metals by either electrowinning or pyrometallurgical means. The most prominent issue is the poor selectivity of the leaching process, which can prolong the procedure, increase the level of chemical additives required and result in associated environmental problems. However, sulfuric acid can offer a solution to the poor leaching selectivity as the very early studies¹⁶⁻¹⁸ show that H₂SO₄ is capable of efficiently separating silver and zinc due to the low solubility of silver and high solubility of zinc in sulfate

media. Furthermore, the sulfuric acid used can also be regenerated by zinc electrowinning via the following reactions:



Despite of the low solubility of silver in sulfuric acid media (≤ 250 ppm),¹⁷ trace amounts of silver can accumulate in the acidic solution after a number of re-use cycles and this results in both a decrease in the level of silver recovered from the batteries, whilst simultaneously having a negative effect on the zinc electrodeposition.

However, the low level of silver in the leaching solutions makes its recovery very challenging. For example, conventional electrowinning (EW) is widely used for silver recovery from concentrated solutions,¹⁹⁻²³ however, in the case of dilute silver solutions, the mass-transport limitation during electrowinning can lead to the dramatic increase of energy consumption and operation time.^{24,25} Various approaches such as ion-exchange,²⁶ membrane separation,²⁷ adsorption²⁸ or solvent extraction²⁹⁻³¹ have been investigated as ways to obtain silver-rich solutions, nevertheless, these methods commonly require the utilization of organic-based substances or extra chemical additions that can result in environmental issues. Additionally, in order to improve the mass transfer process, rotating disk electrodes (RDE) and rotating cylinder electrodes (RCE) have been successfully used to recover silver from low concentration solutions,³²⁻³⁴ however this type of auxiliary equipment also requires extra energy that results in increased operating costs.

Redox replacement reactions are routinely exploited on the laboratory scale by other methods like Surface-Limited Redox Replacement (SLRR) to obtain noble metal mono/multilayers by utilizing underpotential deposition (UDP) of base metals such as nickel,³⁵ lead^{36,37} and copper.³⁸⁻⁴¹ Moreover, redox replacement has also been utilized to produce tailored nanoparticle growth for various catalytic applications.⁴²⁻⁴⁵ Although the redox replacement reaction between silver and other metals have been previously investigated by several researchers, these earlier publications have focused mainly on the morphology and functionality of the products that result from pure solutions with optimized base metal – noble metal concentrations. In contrast, this work utilizes electrodeposition-redox replacement (EDRR) method for silver recovery from realistic solutions with low levels of silver (10 - 100 ppm) that are similar to those found in battery recycling

*Electrochemical Society Member.

^zE-mail: mari.lundstrom@aalto.fi

procedures. EDRR has previously shown great potential for precious metal recovery⁴⁶⁻⁴⁹ but it has not been earlier investigated for silver recovery from battery leaching solutions. In addition, EDRR does not demand any additional chemicals or complex electrical hardware.

Generally, EDRR processes consist of two steps that are then repeated for the desired duration - the first step is the electrodeposition of a sacrificial base metal layer (in this case, Zn). During the second step, the applied potential or current is cut off and the redox replacement between the deposited zinc and silver ions present in solution occurs spontaneously, due to the electrode potential difference between the redox pairs Zn/Zn^{2+} and Ag/Ag^+ . In addition, it is inevitable that fragments of stainless steel from the battery casings will accumulate during a typical button battery crushing-sieving pretreatment process and as Fe is acid soluble, it will also end up into the pregnant leach solution (PLS) generated. In zinc electrowinning, Fe is a traditionally considered as unfavorable element since it can decrease energy efficiency due to the reduction of Fe^{3+} to Fe^{2+} at the cathode and is typically removed prior to zinc electrodeposition.⁵⁰⁻⁵² Consequently - in addition to the recovery of silver from battery leaching solution by EDRR - this research also investigates whether the presence of Fe also has a similar influence on the EDRR process as is observed with EW process.

Experimental

The electrolytes used in the experiments consisted of 60 g·L⁻¹ (0.92 M) Zn^{2+} ($ZnSO_4 \cdot 7H_2O$, ≥ 99%, VWR Chemicals, Belgium), 10 g·L⁻¹ (0.1 M) H_2SO_4 (H_2SO_4 , 95–97%, EMD Millipore, Germany), 100 ppm (0.93 mM) of Ag^+ ($AgNO_3$, ≥ 99.0%, Sigma-Aldrich, USA) and the mimicked effluent solutions from silver oxide button battery recycling processes. Various concentrations of Fe^{3+} ions ($Fe_2(SO_4)_3 \cdot xH_2O$, Fe^{3+} wt% = 22%, $Fe^{2+} \leq 0.03\%$, VWR Chemicals, Belgium) from 0 to 1000 ppm (18 mM) were added to simulate the accumulation of steel case fragments into the solution during the leaching process. All the solutions were prepared with Millipore Milli-Q deionized water (≥ 18 MΩ·cm).

Electrodeposition-redox replacement (EDRR) was conducted in a conventional three- electrode cell (50 cm³) at room temperature. A platinum sheet with a surface area of 0.5 cm² was utilized as the working electrode and another platinum sheet (10 cm²) functioned as the counter electrode (Pt wt% ≥ 99.5%, Kultakeskus Oy, Finland). A saturated mercury-mercurous sulfate electrode (Hg/Hg_2SO_4 , +650 mV vs. Standard Hydrogen Electrode) was used as reference. Prior to the electrochemical deposition process, the platinum sheets were cleaned in 10 g·L⁻¹ H_2SO_4 solution by cycling between -800 mV and +1000 mV vs Hg/Hg_2SO_4 , at a scan rate of 50 mV·s⁻¹ from a starting/end point of -400 mV. After cleaning, the electrodes were thoroughly rinsed with distilled water and dried. All the electrochemical measurements were controlled and monitored using an IviumStat 24-bit CompactStat potentiostat (Ivium Technologies, The Netherlands).

The EDRR process consists of two steps, which were repeated sequentially for a predetermined number (n) of cycles: the first step was the potentiostatic electrodeposition of Zn at E_1 for a predetermined time t_1 , whilst in the second step, the external potential was cut off. The redox replacement reaction spontaneously occurred between Ag^+ ions and the deposited Zn until the potential of the working electrode either reached the pre-defined cutoff potential, E_2 or until a maximum time (1000 s) was achieved. Deposition potential E_1 and the cutoff potential E_2 were selected based on cyclic voltammetry (CV) measurements performed in the silver containing electrolyte solutions and optimized in combination with the deposition time t_1 .

Anodic stripping voltammetry of deposits formed on the working electrodes (WE) was conducted in a solution of 10 g·L⁻¹ H_2SO_4 at a scan speed of 20 mV·s⁻¹ from -400 mV until +500 mV vs. Hg/Hg_2SO_4 in order to determine the amount of recovered silver, A Mira³ Tescan GM (Czech Republic) scanning electron microscope (SEM) equipped with energy-dispersive X-ray spectroscopy (EDS, ThermoFisher Scientific Ultradry EDS Detector, USA) was employed

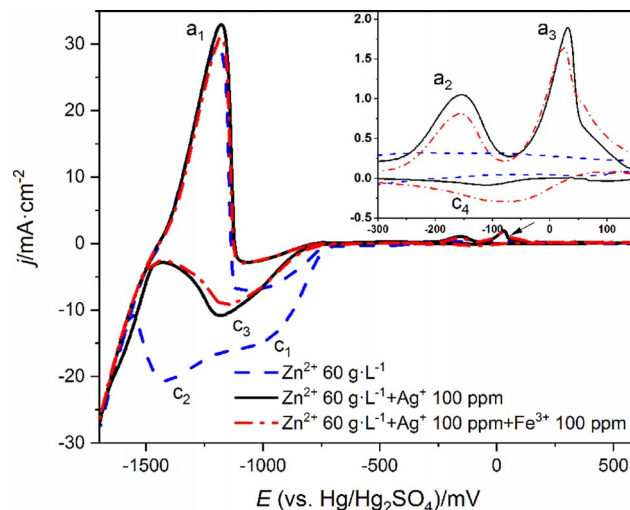


Figure 1. Cyclic voltammograms of Pt electrode recorded in the background solution (60 g·L⁻¹ Zn^{2+} and 10 g·L⁻¹ H_2SO_4), silver-containing solution (60 g·L⁻¹ Zn^{2+} , 10 g·L⁻¹ H_2SO_4 and 100 ppm Ag^+) and the same solution with Fe^{3+} ions (60 g·L⁻¹ Zn^{2+} , 10 g·L⁻¹ H_2SO_4 , 100 ppm Ag^+ and 100 ppm Fe^{3+}) at a scan rate of 20 mV·s⁻¹.

to examine the morphology and composition of the products. All samples were rinsed with deionized water and dried at room temperature prior to analysis. Quantitative analysis of the mass of recovered Ag during different experiments was ascertained via Atomic Absorption Spectroscopy (AAS) after potentiostatic dissolution of the silver deposit (+200 mV vs. Hg/Hg_2SO_4) in a 1 vol % HNO_3 solution (50 cm³).

The specific energy consumption of EDRR (E_s), kWh·kg⁻¹ was calculated with Eq. 3 and Eq. 4:

$$\omega_k = E_{cell} \cdot \int_{t_1} i(t) dt \quad [3]$$

$$E_s = \sum_{k=1}^n \omega_k / m_{Ag} \quad [4]$$

Where E_{cell} is the cell voltage, V, $i(t)$ the function of current with time, A, t_1 is the time duration of electrodeposition step, s, ω_k the energy consumption of k^{th} EDRR cycle, kWh, m_{Ag} is the mass of recovered silver in kg and E_s is the specific energy consumption of n EDRR cycles (kWh·kg⁻¹).

The specific energy consumption (E_s) of the silver electrowinning process in kWh·kg⁻¹ was calculated by Eq. 5 as follows:

$$E_s = E_{cell} \cdot i \cdot t / m_{Ag} \quad [5]$$

Where E_{cell} is the cell voltage, V; i the current, A and t is the electrowinning time duration, s.

The results of E_s are the average values based on triplicate experiments.

Results and Discussion

Cyclic voltammetry studies.—In order to determine the optimum range for the operating parameters (Zn deposition potential, E_1 and cutoff potential for redox replacement step, E_2), cyclic voltammograms were measured in a background solution (60 g·L⁻¹ Zn^{2+} and 10 g·L⁻¹ H_2SO_4), a silver-containing solution (60 g·L⁻¹ Zn^{2+} , 10 g·L⁻¹ H_2SO_4 and 100 ppm Ag^+) and the same silver solution with Fe^{3+} ions (60 g·L⁻¹ Zn^{2+} , 10 g·L⁻¹ H_2SO_4 , 100 ppm Ag^+ and 100 ppm Fe^{3+}), as displayed in Figure 1. Scans commenced from -400 mV (vs. Hg/Hg_2SO_4) in the cathodic direction to a minimum of -1700 mV, it was then reversed to the anodic direction, up to a maximum of +600 mV and before being finally returned back to -400 mV.

Figure 1 shows that in the solution which contained only Zn and sulfuric acid, the hydrogen evolution reaction (HER) commences at around -750 mV, and a small current density plateau (c_1) within the range of HER can be observed at a potential of -800 mV. This is believed to be related to the underpotential deposition (UPD) of zinc and related phenomena, as previously reported Boiadjeva et al.⁵³ As the negative potential is increased, the current density starts to increase rapidly after -1180 mV until a maximum current density is achieved at -1430 mV. After this, the current density starts to decrease, forming a “peak shape” with maximum current density of c_2 . Furthermore around this point a decline in the formation of hydrogen bubbles was also observed - attributed to the initial stages of bulk zinc deposition - as a result of the markedly higher overvoltage of HER on the surface of the formed zinc layer than that of the platinum.⁵⁴ In the positive sweep direction, the deposited zinc is dissolved as indicated by the anodic peak (a_1) starting from -1430 mV.

Clear differences are observed in the presence of Ag^+ ions as the maximum current density in the H_2 evolution area is considerably lower when compared with that of the blank solution. This is believed to be due to the deposited Ag, which is less active toward H_2 evolution than Pt.⁵⁵ In the positive scan, the Zn dissolution process is similar to that without Ag^+ ions, although as the scan goes further, the presence of two anodic peaks is detected. The anodic peak at $+30$ mV (a_3) relates to the stripping of silver, even though the cathodic peak corresponding to silver deposition was not clearly observed due to the relatively low concentration of Ag^+ in solution. It is worth noting that, besides deposition, a strong interaction between deposited zinc and other metals can be established that leads to alloy structure formation^{56–59} and therefore the anodic peak at -150 mV (a_2) can be ascribed to the stripping of a zinc-silver alloy. Addition of 100 ppm Fe^{3+} has only minor influence on the shape of CV curves; the appearance of a peak at -100 mV relates to the reduction reaction of the $\text{Fe}^{3+}/\text{Fe}^{2+}$ redox pair, while the anodic counterpart overlaps with the silver stripping peak due to the similar standard potential values of $\text{Fe}^{3+}/\text{Fe}^{2+}$ (-771 mV vs SHE) and Ag^+/Ag (-800 mV vs. SHE).⁶⁰

Based on the CV studies, in order to obtain a sacrificial zinc deposit, the first steps of EDRR- zinc electrodeposition should be performed at a potential (E_1) that is more negative than -1430 mV, whilst the cutoff potential (E_2) should be set to be around -100 mV vs. $\text{Hg}/\text{Hg}_2\text{SO}_4$. It is noteworthy, that during the redox replacement step, the potential observed as a function of time relates to the open circuit potential (OCP). This changes as the Zn-rich electrode transforms to a Ag-rich electrode, due to spontaneous redox replacement reaction between deposited Zn and Ag^+ ions present in solution. Therefore the cutoff potential (i.e. the potential which OCP needs to reach before the next electrodeposition step can start) should be sufficiently anodic to ensure a higher purity deposit but not anodic enough to reach the silver stripping region.

Electrodeposition-redox replacement.—Figure 2 shows a typical potential-time and current-time curves selected from a 20-cycle EDRR process. Both curves show the application of the deposition voltage ($E_1 = -1500$ mV for 5 s) which is immediately followed by the absence of any applied external potential and subsequently results in changes to the open circuit potential (OCP) during the redox replacement step. The open circuit potential (OCP) increases toward the anodic direction with the change in deposit composition on the electrode surface until the OCP reaches -100 mV (i.e. the pre-determined cutoff potential E_2) and the next cycle can commence. The driving force of the redox replacement reaction is the potential difference that exists between the redox pairs Ag^+/Ag and Zn^{2+}/Zn . From the typical time-current transient curve of the deposition step of a single cycle, it can be seen that a sharp decrease occurs in the initial stage that can be attributed to electrochemical double layer charging followed by the nucleation process.^{61,62}

EDRR parameter optimization.—Immediately after EDRR cycling, the sample was removed from the solution, rinsed with deionized water and dried. The sample was subsequently placed in H_2SO_4 so-

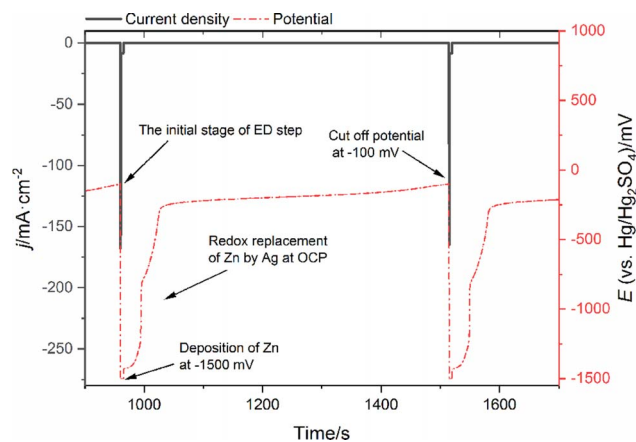


Figure 2. Time-Current-Potential graph illustrating one EDRR cycle. Zn is deposited at -1500 mV and then replaced by Ag^+ ions at open circuit potential (OCP). The EDRR cycle ends when OCP reaches the cutoff potential -100 mV vs. $\text{Hg}/\text{Hg}_2\text{SO}_4$ and next cycle follows. (Solution composition: $60 \text{ g}\cdot\text{L}^{-1} \text{Zn}^{2+}$, $10 \text{ g}\cdot\text{L}^{-1} \text{H}_2\text{SO}_4$, 100 ppm Ag^+ and 100 ppm Fe^{3+}).

lution and a CV was measured in the anodic range in order to detect the anodic stripping peak of Ag. This stripping peak was utilized as a marker of successful Ag recovery and was used for the optimization of the EDRR parameters (E_1 , E_2 and t_1).

In this study, two different electrodeposition potentials were investigated: a potential close to the zinc deposition potential (-1500 mV) and another with a higher deposition overpotential (-1600 mV). In all of these experiments, a cutoff potential (E_2) of -100 mV was employed. To determine the optimum deposition time for a single cycle, 100 seconds of total deposition time was applied in all experiments. In this case, the deposition time t_1 for a single EDRR cycle was selected as 1 s, 2.5 s, 5 s, 10 s and 20 s, resulting in a total cycle number of 100 , 40 , 20 , 10 and 5 , respectively. All the measurements for parameter optimization were carried out in a solution containing $60 \text{ g}\cdot\text{L}^{-1} \text{Zn}^{2+}$, $10 \text{ g}\cdot\text{L}^{-1} \text{H}_2\text{SO}_4$, 100 ppm Ag^+ and 100 ppm Fe^{3+} .

Figure 3 shows the stripping peaks in a $10 \text{ g}\cdot\text{L}^{-1} \text{H}_2\text{SO}_4$ solution measured immediately after the EDRR experiments (EDRR parameters: deposition potential E_1 of -1500 mV and cutoff potential E_2 of -100 mV) with varying deposition times t_1 . It can be seen that the peak current rises slightly with the increase in t_1 over the range of 1 s

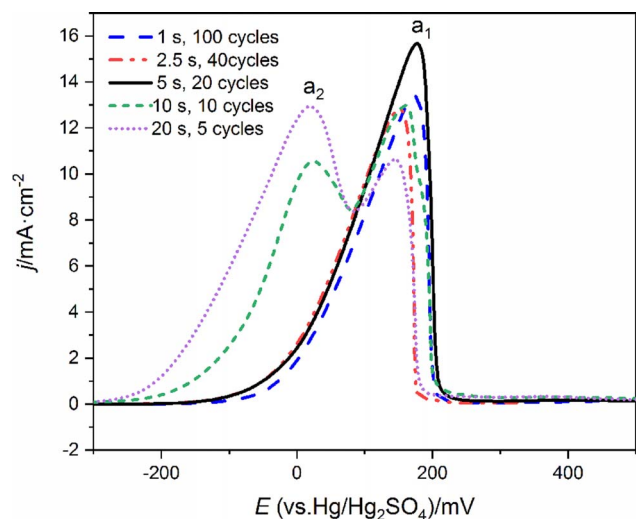


Figure 3. Anodic stripping voltammetry of Ag on WE in a $10 \text{ g}\cdot\text{L}^{-1} \text{H}_2\text{SO}_4$ after EDRR experiments at a deposition potential E_1 of -1500 mV with varying deposition time t_1 . Scan rate = $20 \text{ mV}\cdot\text{s}^{-1}$. (Solution composition of EDRR: $60 \text{ g}\cdot\text{L}^{-1} \text{Zn}^{2+}$, $10 \text{ g}\cdot\text{L}^{-1} \text{H}_2\text{SO}_4$, 100 ppm Ag^+ and 100 ppm Fe^{3+}).

Table I. SEM-EDS quantitative results of product composition on WE surface after EDRR experiments at E_1 of -1500 mV and E_2 of -100 mV with varying deposition time t_1 (average value of 15 point/area spectra, where the background signal Pt (wt%) is excluded).

Deposition time(s)	Number of cycles	Ag (wt%)	Zn (wt%)	Fe (wt%)	Ag/Zn
1	100	38.9 ± 1.3	1.6 ± 0.6		24.3
2.5	40	40.1 ± 1.1	1.7 ± 0.7		23.5
5	20	43.5 ± 0.8	2.3 ± 0.6	N/A	18.9
10	10	32.6 ± 1.2	14.8 ± 2.1		2.2
20	5	28.9 ± 2.1	17.7 ± 1.1		1.6

to 5 s, indicating that longer deposition times are more favorable for silver recovery. This is due to the fact that a combination of a short deposition time with the increased number of cycles, overall, consumes more charge for the double layer charging during the initial stages of ED step than for the actual Zn deposition. Consequently, the amount of zinc deposited decreases as conversely the level of energy consumption increases, which in turn lowers the amount of silver recovered via redox replacement. On the other hand, when t_1 exceeds 10 s, the stripping peaks possess a double-peak characteristic, of which the anodic peak a_2 corresponds to the dissolution of zinc from zinc-silver alloy due to incomplete redox replacement. The SEM-EDS results present in Table I, analyzed after EDRR measurements, support this variation in purity with different deposition time. The deposit on the electrode surface obtained with $t_1 = 5$ s of has the highest yield and a favorable purity. It is also worth noting that no impurity Fe is observed on the electrode surface.

Figure 4 shows the stripping peaks obtained at a deposition potential of -1600 mV and it can be seen that the results are similar to those obtained at $E_1 = -1500$ mV. The highest silver amount recovered was achieved with a deposition time $t_1 = 2.5$ s whereas longer t_1 (≥ 5 s) again leads to incomplete redox replacement and a degradation of deposit quality. Comparison of the results achieved at the respective optimum deposition times ($E_1 = -1500$ mV, $t_1 = 5$ s and $E_1 = -1600$ mV, $t_1 = 2.5$ s), shows that the stripping current amplitude at -1600 mV ($j_{max} = 20.7$ mA·cm $^{-2}$) is slightly higher than that of -1500 mV ($j_{max} = 15.6$ mA·cm $^{-2}$). Nonetheless, it is worth noting that during Zn deposition, HER is inevitable,⁶³ and as higher overvoltage can cause an increase of energy consumption due to HER, the lowest possible overvoltage is typically considered to be the most favorable for the ED step. The SEM micrographs, displayed in Figure 5, indicate that the deposition potential has a significant

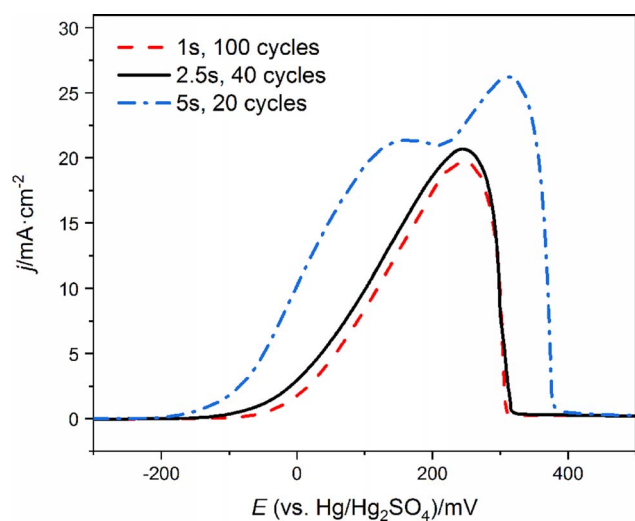


Figure 4. Anodic stripping voltammetry of Ag on WE measured in a 10 g·L $^{-1}$ H $_2$ SO $_4$ after EDRR experiments (EDRR parameters: E_1 of -1600 mV and E_2 of -100 mV with varying deposition time t_1). Scan rate = 20 mV·s $^{-1}$. (Solution composition of EDRR: 60 g·L $^{-1}$ Zn $^{2+}$, 10 g·L $^{-1}$ H $_2$ SO $_4$, 100 ppm Ag $^+$ and 100 ppm Fe $^{3+}$).

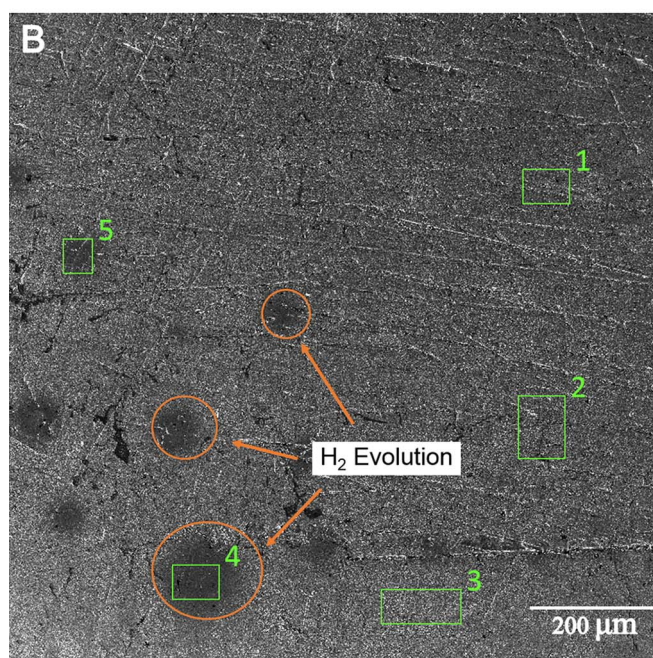
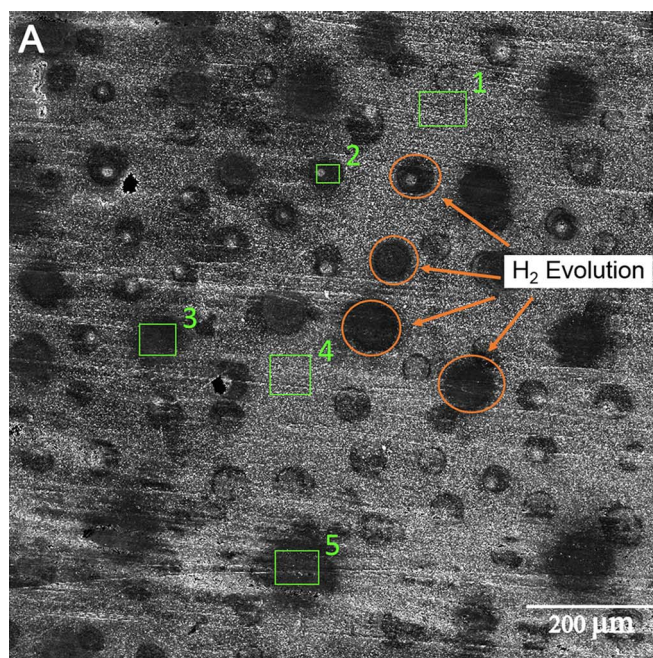


Figure 5. SEM micrographs of WE after n cycles of EDRR experiment at different deposition potential E_1 with optimum deposition time t_1 . (A) $E_1 = -1600$ mV, $t_1 = 2.5$ s, $E_2 = -100$ mV, $n = 40$ cycles; (B) $E_1 = -1500$ mV, $t_1 = 5$ s, $E_2 = -100$ mV, $n = 20$ cycles. (Solution composition of EDRR: 60 g·L $^{-1}$ Zn $^{2+}$, 10 g·L $^{-1}$ H $_2$ SO $_4$, 100 ppm Ag $^+$ and 100 ppm Fe $^{3+}$).

Table II. Comparison of SEM-EDS quantitative results of product composition on WE surface after EDRR experiments at different deposition potentials, E_1 (the background signal Pt (wt%) is excluded).

E_1	Spectrum number	Ag (wt%)	Zn (wt%)	Fe (wt%)	Ag/Zn
-1600 mV	1	55.7	3.5		15.9
	2	0.5	0.1		5
	3	1.1	0.2		5.5
	4	59.2	5.1		12.7
	5	0.3	0.1		3
-1500 mV	1	43.1	2.3	N/A	18.7
	2	48.2	2.9		16.6
	3	47.6	2.1		22.7
	4	25.5	1.3		19.6
	5	31.2	1.2		26

impact on surface morphology. The distinct, dark colored spots (showing mostly the underlying WE) observed after EDRR at the E_1 of -1600 mV (Figure 5A) are attributed to intensive H_2 bubble formation, while the surface uniformity after EDRR at E_1 of -1500 mV (Figure 5B) shows that it is only mildly affected by HER. Moreover, the corresponding EDS results shown in Table II also suggest that $E_1 = -1500$ mV is more favorable than -1600 mV. Although the spectra outside the dark colored surface area have a higher content of Ag at the more negative potential (-1600 mV), the purity (Ag/Zn ratio) is lower than that obtained at -1500 mV. Based on these observations, the optimum parameters for ED step is selected as $E_1 = -1500$ mV and $t_1 = 5$ s.

Optimization of cutoff potential E_2 was conducted over a potential range from -80 mV to -130 mV (stripping peaks shown in Figure 6). It can be seen that even a slight change of cutoff potential has a noticeable influence. The lowest current density in the stripping peak area of silver is obtained at an E_2 of -80 mV, indicating that a too positive cutoff potential ($E_2 = -80$ mV) decreases the silver recovery due to the dissolution of deposited silver, whereas the double-peak shape acquired at $E_2 = -130$ mV suggests that when cutoff potential is too negative, it degrades the product purity due to incomplete replacement of the zinc-silver alloy. Consequently, the optimum cutoff

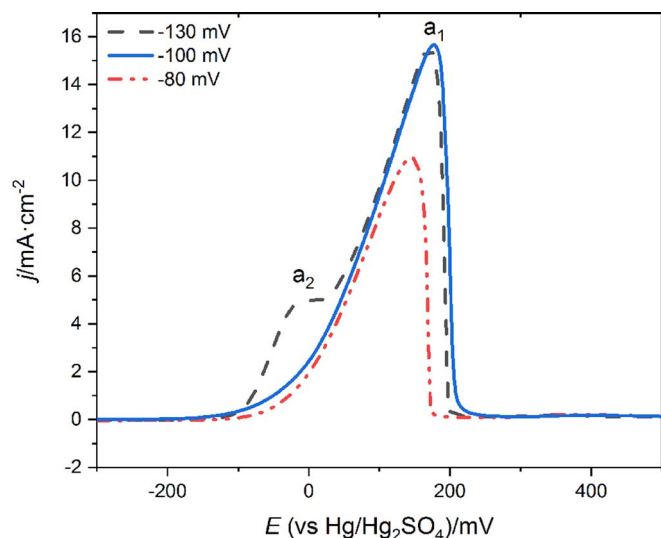


Figure 6. Anodic stripping voltammograms of Ag on WE in a 10 g·L⁻¹ H₂SO₄ after EDRR experiments at deposition potential E_1 of -1500 mV, deposition time t_1 of 5 s and varying cutoff potential E_2 . Scan rate = 20 mV·s⁻¹. (Solution composition of EDRR: 60 g·L⁻¹ Zn²⁺, 10 g·L⁻¹ H₂SO₄, 100 ppm Ag⁺ and 100 ppm Fe³⁺).

Table III. SEM-EDS quantitative results of product composition on WE surface after EDRR experiments at different cutoff potentials, E_2 (average value of 15 point/area spectra, where the background signal Pt (wt%) is excluded).

E_2 /mV	Ag (wt%)	Zn (wt%)	Fe (wt%)	Ag/Zn
-130	41.8 ± 2.3	9.8 ± 1.4		4.3
-100	43.5 ± 1.6	2.3 ± 0.6	N/A	18.9
-80	27.6 ± 0.9	1.3 ± 0.6		21.3

potential was selected as -100 mV, a level which is further confirmed by the corresponding SEM-EDS results shown in Table III.

Effect of EDRR cycles.—The effect of repeating EDRR cycles n (from 20 to 100) on silver recovery was investigated with electrolytes containing 100 ppm Ag⁺, 60 g·L⁻¹ Zn²⁺, 100 ppm Fe³⁺ and 10 g·L⁻¹ H₂SO₄ ($E_1 = -1500$ mV, $t_1 = 5$ s and $E_2 = -100$ mV).

Anodic stripping curves after EDRR experiments are shown in Figure 7 and the marked rise in peak height with repeated cycles shows an increase in the silver yield. In contrast, presence the Zn peak is not detected in any of the curves, which indicates that the product quality is not degraded by the increase in the number of cycles. This is also confirmed by the SEM-EDS results outlined in Table IV. Although there is a slight fluctuation of product quality (in terms of Ag/Zn ratio) with the different number of EDRR cycles, after 100 cycles of EDRR the variation in product quality is negligible, which indicates the feasibility of long term operation. Deposit morphology after different EDRR cycles are shown in Figure 8. As can be seen, the silver is initially enriched on the defects within the platinum substrates (i.e. the dots with light color shown in Figure 8A), as areas with a higher surface energy are preferable for zinc nucleation.⁶⁴ With an increase in the number of cycles, the grain size increases and dendritic style crystals start to grow on the top of some grains (Figure 8B) and after sufficient cycles a more continuous phase of these dendrites is formed (Figure 8C).

Effect of the iron impurity.—Iron dissolution is also likely to occur in button battery leaching due to the presence of steel battery casing scraps and therefore, the change in silver recovery with varying concentrations of Fe³⁺ ions (ranging from 0 to 1000 ppm) was

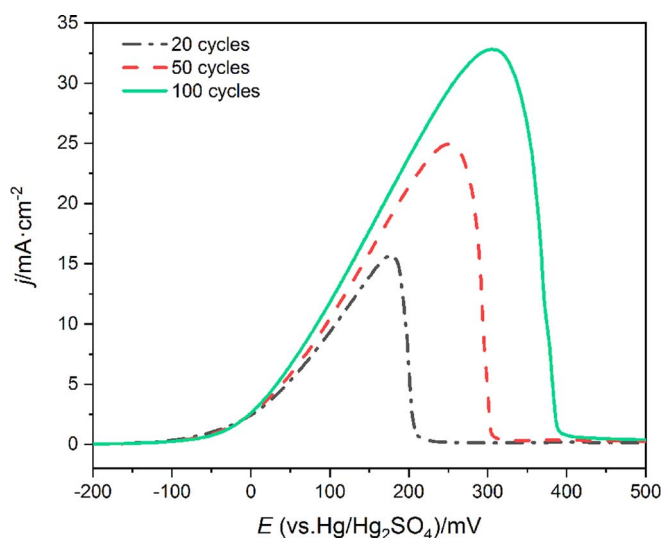


Figure 7. Anodic stripping voltammograms of Ag on WE in a 10 g·L⁻¹ H₂SO₄ after EDRR experiments at deposition potential E_1 of -1500 mV, deposition time t_1 of 5 s, cutoff potential E_2 of -100 mV and varying cycles. Scan rate = 20 mV·s⁻¹. (Solution composition of EDRR: 60 g·L⁻¹ Zn²⁺, 10 g·L⁻¹ H₂SO₄, 100 ppm Ag⁺ and 100 ppm Fe³⁺).

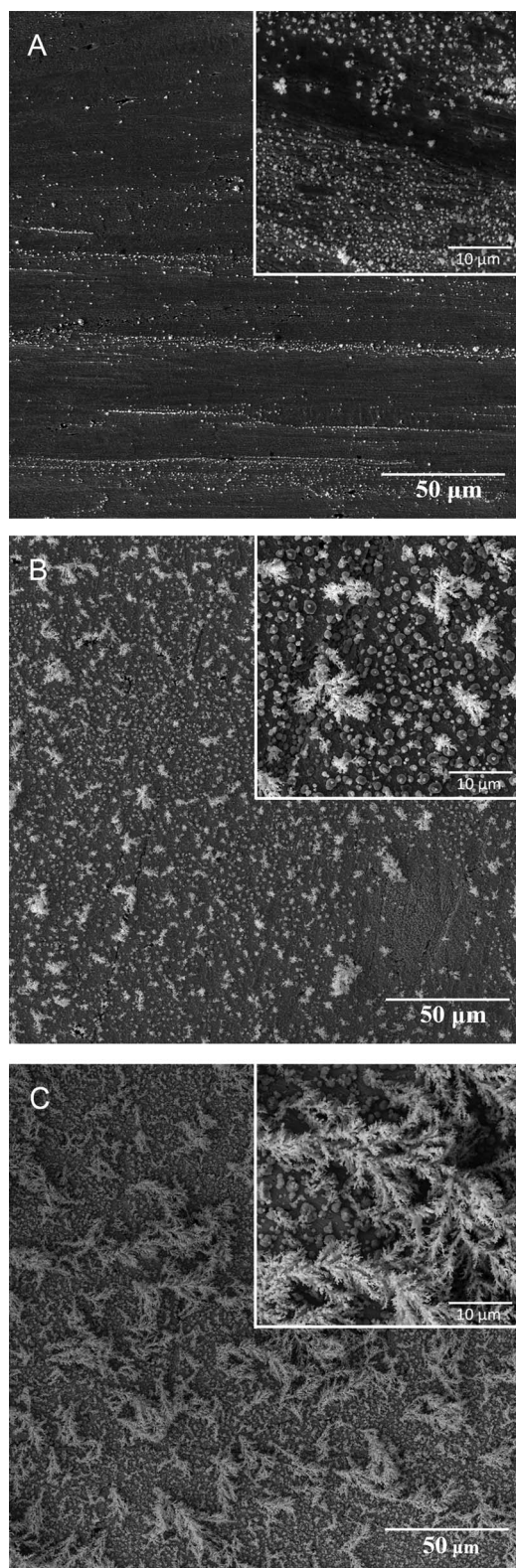


Figure 8. SEM micrographs after EDORR experiments at deposition potential E_1 of -1500 mV, deposition time $t_1 = 5$ s, cutoff potential $E_2 = -100$ mV for different cycles. (A) $n = 20$ cycles; (B) $n = 50$ cycles; (C) $n = 100$ cycles. (Solution composition: $60 \text{ g}\cdot\text{L}^{-1} \text{ Zn}^{2+}$, $10 \text{ g}\cdot\text{L}^{-1} \text{ H}_2\text{SO}_4$, 100 ppm Ag^+ and 100 ppm Fe^{3+}).

Table IV. SEM-EDS quantitative results of product composition on WE surface after EDORR experiments at different number of cycles, n (average value of 15 point/area spectra, where the background signal Pt (wt%) is excluded).

Cycles/ n	Ag (wt%)	Zn (wt%)	Fe (wt%)	Ag/Zn
20	43.5 ± 1.8	2.3 ± 0.4		18.9
50	65.8 ± 1.3	4.1 ± 1.1	N/A	16.3
100	82.7 ± 2.2	4.1 ± 0.8		20.1

investigated with electrolytes containing 100 ppm Ag^+ , $60 \text{ g}\cdot\text{L}^{-1} \text{ Zn}^{2+}$ and $10 \text{ g}\cdot\text{L}^{-1} \text{ H}_2\text{SO}_4$. The EDORR experiments were repeated for 20 cycles under the abovementioned optimized operating parameters ($E_1 = -1500$ mV, $t_1 = 5$ s and $E_2 = -100$ mV).

The anodic stripping curves after EDORR experiments are shown in Figure 9. The peak amplitude clearly demonstrates the effect of initial Fe^{3+} concentration on the silver recovery by EDORR. Low level additions (10 ppm) of Fe^{3+} ions only have a minor influence on the resultant stripping peaks, however, when the Fe concentration is increased from 100 ppm to 1000 ppm , a dramatic decrease in the level of silver recovery takes place, which is believed to result from the simultaneous reduction of $\text{Fe}^{3+}/\text{Fe}^{2+}$ during Zn electrodeposition. Furthermore, this competing $\text{Fe}^{3+}/\text{Fe}^{2+}$ reduction process can also consume some of the Zn deposited on the electrode surface. Nevertheless, it is also worth noting that when these EDORR results are compared to those for zinc electrowinning in the literature⁵⁰ - where an Fe ion concentration of only 20 ppm is known to drastically decrease energy efficiency - it can be seen that despite of the presence of Fe ions, the EDORR method could still be successfully utilized at an Fe^{3+} concentration of 1000 ppm for Ag recovery.

The trend indicated by the stripping peak analysis is also confirmed by SEM analysis (Table V). With 10 ppm of Fe^{3+} , the silver amount obtained decreases only slightly but a more dramatic decrease is observed when the Fe addition exceeds 100 ppm , which is in agreement with the anodic stripping curves. Nonetheless, in spite of high Fe ion concentrations in solution, Ag is clearly predominates within the deposit, whilst Zn content only varies between 0.1 and 3.9% . Additionally, Fe is not detected in the product in any of the experiments, although the redox pair Fe^{2+}/Fe has a more positive potential than that

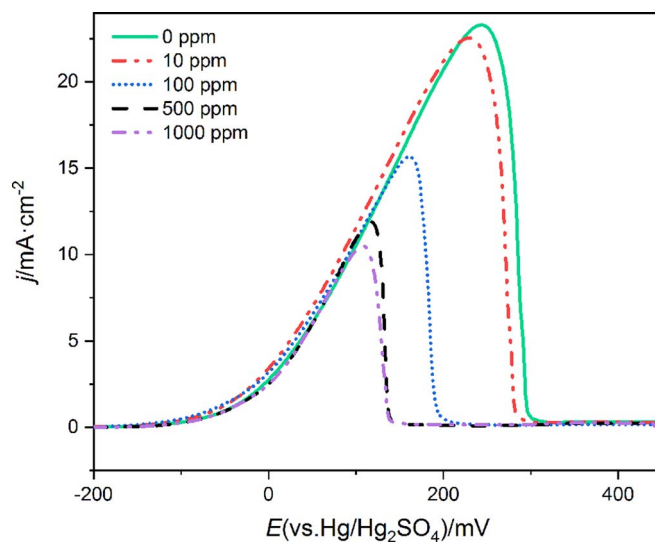


Figure 9. Anodic stripping voltammetry of Ag on WE in a $10 \text{ g}\cdot\text{L}^{-1} \text{ M H}_2\text{SO}_4$ after EDORR experiments ($E_1 = -1500$ mV, $t_1 = 5$ s, $n = 20$ cycles and $E_2 = -100$ mV) with electrolytes containing 100 ppm Ag^+ , $60 \text{ g}\cdot\text{L}^{-1} \text{ Zn}^{2+}$, $10 \text{ g}\cdot\text{L}^{-1} \text{ H}_2\text{SO}_4$ and varying Fe^{3+} concentration from 0 to 1000 ppm . Scan rate = $20 \text{ mV}\cdot\text{s}^{-1}$.

Table V. Comparison of SEM-EDS quantitative results of product composition on WE surface after EDRR experiments, in solutions with different Fe impurity contents (average value of 15 point/area spectra and the background signal Pt (wt%) is excluded).

Initial Fe ³⁺ concentration/ppm	Ag (wt%)	Zn (wt%)	Fe (wt%)	Ag/Zn
0	55.6 ± 1.1	3.9 ± 0.5		14.1
10	52.1 ± 0.8	3.8 ± 0.9		13.5
100	43.5 ± 1.4	2.3 ± 0.6	N/A	18.9
500	28.2 ± 0.7	1.2 ± 0.3		23.5
1000	22.5 ± 0.4	0.8 ± 0.4		28.1

of Zn²⁺/Zn, which indicates that the presence of Fe impurities in the electrolyte has no effect on the final deposit quality.

Naturally, the competing Fe³⁺/Fe²⁺ reduction takes place during the redox replacement step as well but with the EDRR method it appears to have a small beneficial effect (Table IV). This is demonstrated by the purity of the deposit (in terms of Ag/Zn ratio) which is higher when Fe is present in solution, due to the spontaneous oxidation of Zn by Fe³⁺ which improves the Ag purity. A comparison of the EDRR process in the presence and absence of Fe³⁺ is shown schematically in Figure 10. In the case further purifications are needed for the recovered silver product, electrorefining could be a possible option as it is widely used in the industrial scale.

Comparison between EDRR and electrowinning (EW).—In order to demonstrate the true potential of EDRR, a comparison between EW (which is widely used for industrial silver recovery) and EDRR is performed (Figure 11), both from the recovered silver amount and energy consumption points-of-view. Figure 11A shows the differences in amplitude (j_{max}) of the anodic stripping peaks - which is directly related to the amount of Ag recovered - as a function of Fe³⁺ concentration. The EW experiments were conducted at -300 mV (vs. Hg/Hg₂SO₄) and the deposition time for EW used (300 s) was 3 times higher than the total duration of the 20 ED steps in EDRR process; N.B. if the same deposition times were used, the Ag amount recovered by EW is insufficient to produce detectable stripping peaks. It can be seen that the height of the silver anodic stripping peaks obtained via EDRR are markedly higher than those achieved with EW, especially at low Fe electrolyte content (≤ 100 ppm). Therefore it can be concluded that the presence of Fe decreases the yield of the both processes, and

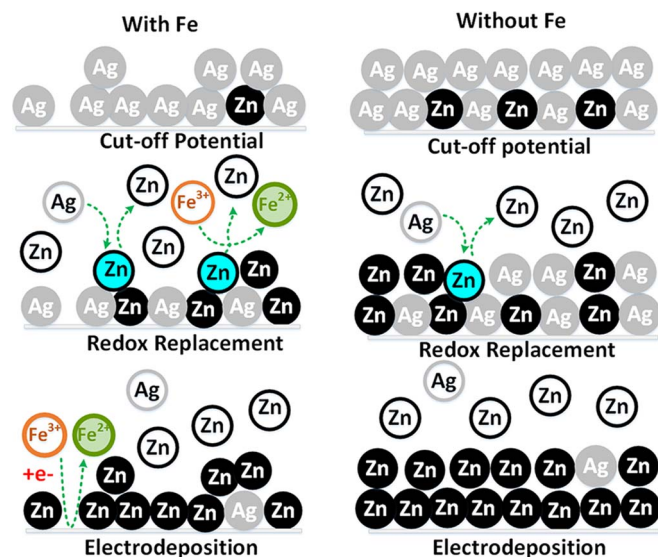


Figure 10. Schematic illustrating the progress of electrodeposition-redox replacement in zinc solution containing silver in the presence/absence of Fe³⁺.

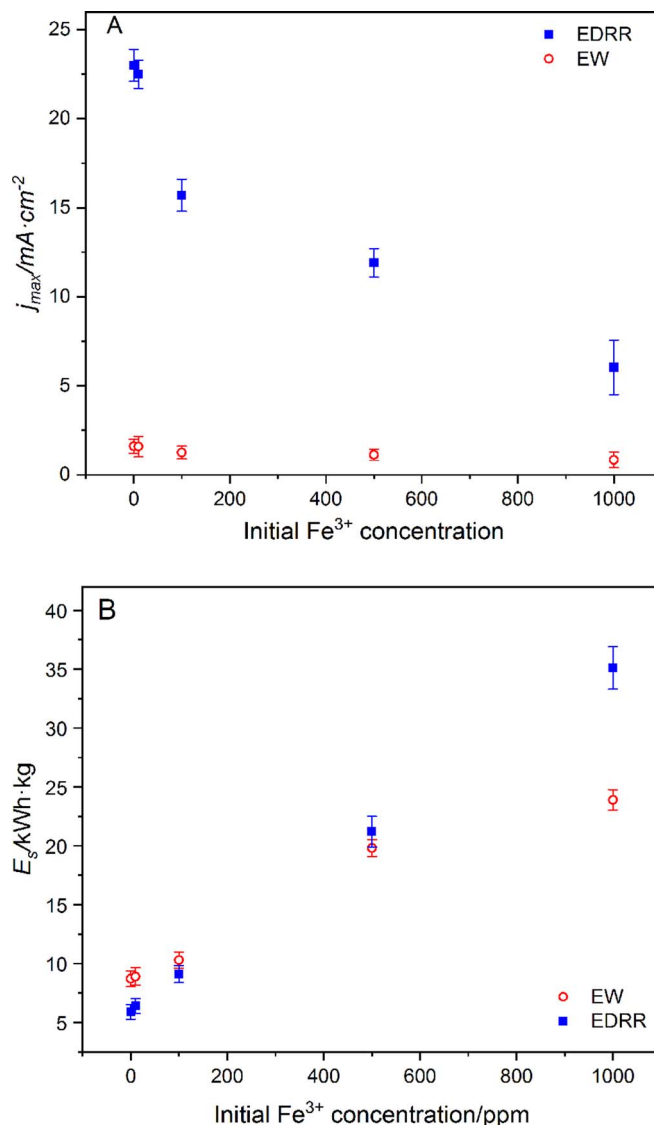


Figure 11. Comparison of stripping peak height and E_s after EDRR ($E_1 = -1500$ mV, $t_1 = 5$ s, $n = 20$ cycles and $E_2 = -100$ mV vs. Hg/Hg₂SO₄) and EW ($E = -300$ mV vs. Hg/Hg₂SO₄ and $t = 300$ s) in electrolytes containing 100 ppm Ag⁺, 60 g·L⁻¹ Zn²⁺, 10 g·L⁻¹ H₂SO₄ and varying Fe³⁺ content from 0 to 1000 ppm.

it is significant that even with a Fe concentration of 1000 ppm, the peak height obtained with EDRR is still much higher than that of EW, clearly showing the advantage of EDRR over EW in terms of silver yield.

In addition, the specific energy consumption (E_s) per kilogram of silver deposited (kWh·kg⁻¹) was calculated by Eq. 3, Eq. 4 and Eq. 5 and comparison between EW and EDRR is shown in Fig. 11B. As the deposition step of EDRR is potentiostatic, there is a sharp increase in current during the initial stages, due to the electrochemical double layer charging and subsequent nucleation process. This effect is not negligible in the EDRR method, especially in the situation where there are short deposition steps which are repeated a number of times. As a result, the energy consumption for a single EDRR cycle is calculated by multiplying the cell voltage (E_{cell}) with charge consumption (the integration of current during deposition time t_1) and the E_s of EW is calculated by multiplying the cell voltage E_{cell} with the current i and time t , the results of which are shown in Figure 11B.

It can be seen from Figure 11 that the E_s of both EDRR and EW increases with the increasing Fe concentration and the EDRR is more

Table VI. Composition of silver oxide button battery pregnant leaching solution (PLS).

Species	Ag (ppm)	Zn (g·L ⁻¹)	Fe (ppm)	H ₂ SO ₄ (g·L ⁻¹)
Concentration	63	64.8	166	14.3

sensitive to the presence of Fe ions. The E_s of EDRR is lower than that of EW at low Fe concentrations (< 100 ppm), and the lower the Fe content, the higher the difference. For example, at a Fe concentration of 10 ppm, the E_s of EDRR is 2.5 kWh·kg⁻¹ lower than EW. On the other hand at a concentration range between 100 – 500 ppm, both methods have a relatively similar energy consumption, whilst EDRR consumes more energy than EW when the concentration of Fe ion exceeds 500 ppm. Although this indicates that EDRR may have an energy efficiency limit when applied industrially, this can be easily overcome by use of a Fe removal procedure for electrolyte solutions with high levels of Fe impurities - as is already typically done in industrial zinc EW processes - prior to EDRR.

Silver recovery via EDRR from leaching solution of silver button battery.—The applicability of the EDRR method for silver recovery was finally tested with real pregnant leaching solutions (PLS) of silver oxide button batteries containing lower levels of silver and higher impurity Fe levels (Table VI). Figure 12 shows the stripping peaks after varying cycles of EDRR in silver oxide button batteries PLS. The single peak shape of the stripping peaks and the increasing peak height with cycle numbers indicate the successful recovery of silver. Additionally, the recovery efficiency (%) of silver was determined by AAS and the results are presented in Table VII. As it can be seen, the recovery efficiency of silver is increased rather linearly with number of cycles, reaching nearly 70% after 300 cycles of EDRR. Furthermore it is noteworthy that as the EDRR process showed a great stability as a function of cycles (section Effect of EDRR cycles), the recovery efficiency could be further improved by increasing the cycle number.

The morphology of the deposits are shown in Figure 13A, and it differs from the morphology observed in deposits from synthetic solution, most likely due to the minor concentration of other impurities: in real solution the morphology is agglomerated particles while in synthetic solution a more dendritic growth was observed. In order to further verify the feasibility of EDRR on the industrial scale, a more economical electrode material — glassy carbon - was tested. The SEM micrographs of the glassy carbon electrode after EDRR in silver

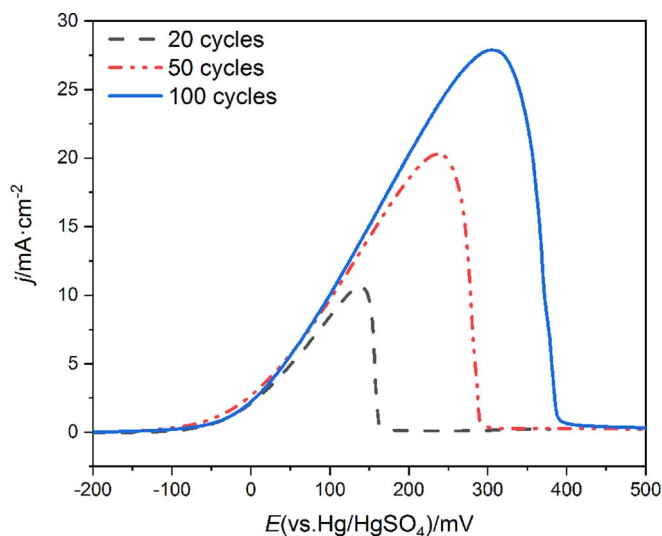


Figure 12. Anodic stripping voltammetry of Ag on WE in a 10 g·L⁻¹ M H₂SO₄ after varying cycles of EDRR experiments ($E_I = -1500$ mV, $t_I = 5$ s, and $E_2 = -100$ mV) with real silver oxide battery PLS. Scan rate = 20 mV·s⁻¹.

Table VII. The silver recovery efficiency from silver oxide button battery pregnant leaching solution (PLS) as a function of EDRR cycles.

Cycles (n)	50	100	150	300
Recovery efficiency (%)	15.3 ± 3.7	27.9 ± 2.5	40.8 ± 4.5	68.5 ± 6.8

button battery PLS are presented in Figure 13B. The correlated EDS results in Table VIII indicate the successful recovery on both platinum electrode and glassy carbon electrode, showing again the versatility of EDRR process when it comes to the recovery of trace elements from real leaching solutions.

Conclusions

In summary, the recovery of silver from the dilute effluents from silver oxide battery recycling process with low silver content (100 ppm) by electrodeposition-redox replacement (EDRR) has been studied. The effects of the operating parameters, including deposition potential, deposition time and cutoff potential on the silver yield and product composition were investigated. Optimum conditions for the EDRR process in a solution containing 100 ppm Ag⁺, 100 ppm Fe³⁺, 60 g·L⁻¹ Zn²⁺ and 10 g·L⁻¹ H₂SO₄ are as follows: a deposition

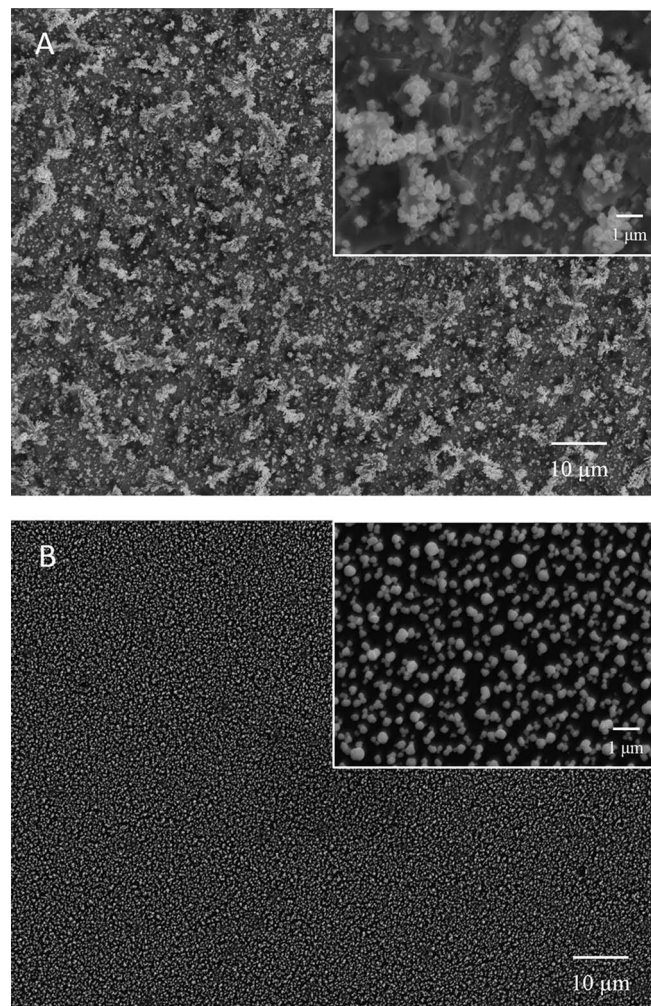


Figure 13. SEM micrographs of WE after 50 cycles of EDRR experiment ($E_I = -1500$ mV, $t_I = 5$ s, and $E_2 = -100$ mV) in real silver oxide battery PLS: A) platinum electrode; B) glassy carbon electrode.

Table VIII. SEM-EDS quantitative results of product composition via EDRR from real silver oxide button cell leaching solution (PLS) on platinum electrodes and glassy carbon electrodes (average value of 15 point/area spectra, where the background signals Pt (wt%) and C (wt%) are excluded).

Electrode Material	EDRR Cycles (<i>n</i>)	Ag (wt%)	Zn (wt%)	Fe (wt%)	Ag/Zn
Platinum	50	54.6 ± 2.1	2.5 ± 0.3	N/A	21.8
Glassy Carbon	50	49.2 ± 1.7	3.1 ± 0.6		15.9

potential of -1500 mV vs. $\text{Hg}/\text{Hg}_2\text{SO}_4$, deposition time for a single EDRR cycle of 5 s and cutoff potential of -100 mV. The dissolution of steel may also take place during the battery recycling, resulting in the presence of Fe ions impurities in solution. In this study it was observed that increasing Fe concentrations can have a noticeable impact on the silver yield due to the redox behavior of $\text{Fe}^{3+}/\text{Fe}^{2+}$ pair during the Zn deposition and the competing reduction during redox replacement. Although this may consequentially reduce the amount of Ag recovered, it also results in an improvement in product quality in terms of the Zn:Ag ratios. The specific energy consumption (E_s) of EDRR was compared to traditional electrowinning (EW) and was determined to be lower for EDRR at low Fe ion content (0–100 ppm). Furthermore, EDRR was also found to significantly improve the silver yield when compared to the conventional electrowinning process, even with Fe levels of 1000 ppm. In addition to this, the EDRR process was tested also for more industrially relevant conditions, i.e. using real silver oxide battery leaching solutions and glassy-carbon electrodes. Based on these results, it can be concluded that EDRR is a competitive method for the recovery of silver from sulfate media with low Ag concentrations.

Acknowledgments

This research has been financed by the Academy of Finland, NoWaste project (grant No. 297962, authors: ZW, KY), GoldTail (grant No. 319691, author: BP) and the Association of Finnish Steel and Metal Producers (METSEK-project, author: PH). BATCircle (grant No. 4853/31/2018) funded by Business Finland is acknowledged by ML. The RawMatTERS Finland Infrastructure (RAMI) funded by Academy of Finland and based at Aalto University is also acknowledged. In addition, Zulin Wang thanks the Chinese Scholarship Council (CSC) for their support.

ORCID

Zulin Wang  <https://orcid.org/0000-0002-2234-7983>
 Petteri Halli  <https://orcid.org/0000-0002-1803-7632>
 Pyry Hannula  <https://orcid.org/0000-0001-9844-2234>
 Benjamin P. Wilson  <https://orcid.org/0000-0002-2874-6475>
 Kirsi Yliniemi  <https://orcid.org/0000-0003-2536-388X>
 Mari Lundström  <https://orcid.org/0000-0002-6655-6779>

References

- F. Liu, J. Wang, C. Peng, Z. Liu, B. P. Wilson, and M. Lundström, *Hydrometallurgy*, **185**, 38 (2019).
- P. R. Norris, L. Laigle, T. J. Ogdan, and O. J. P. Gould, *Miner. Eng.*, **106**, 7 (2017).
- X. Li, Y. Wang, X. Cui, Z. Lou, W. Shan, Y. Xiong, and Y. Fan, *Hydrometallurgy*, **176**, 192 (2018).
- C. Rodríguez-Rodríguez, F. Nava-Alonso, A. Uribe-Salas, and J. Viñals, *Hydrometallurgy*, **164**, 15 (2016).
- H. Sverdrup, D. Koca, and K. V. Ragnarsdóttir, *Resour. Conserv. Recycl.*, **83**, 121 (2014).
- K. Liu, Z. Zhang, and F.-S. Zhang, *J. Hazard. Mater.*, **318**, 216 (2016).
- P.-P. Sun, H.-I. Song, T.-Y. Kim, B.-J. Min, and S.-Y. Cho, *Ind. Eng. Chem. Res.*, **53**, 20241 (2014).
- A. D. Bas, E. Y. Yazici, and H. Deveci, *Hydrometallurgy*, **121–124**, 22 (2012).
- Z. Gamiño-Arroyo, A. Tapiá-Cisneros, O. M. Zamacona-Saucedo, I. Cano-Rodríguez, A. F. Aguilera-Alvarado, L. E. Sánchez-Cadena, and F. I. Gómez-Castro, *J. Mater. Sci. Chem. Eng.*, **03**, 148 (2015).
- U. Jadhav, C.-H. Su, M. Chakankar, and H. Hocheng, *DEStech Trans. Eng. Technol. Res.*, 0 (2017).
- S. Aktas, *Hydrometallurgy*, **104**, 106 (2010).
- N. Sathaiyan, V. Nandakumar, and P. Ramachandran, *J. Power Sources*, **161**, 1463 (2006).
- U. Jadhav and H. Hocheng, *J. Clean. Prod.*, **44**, 39 (2013).
- U. Jadhav, C.-H. Su, M. Chakankar, and H. Hocheng, *Batteries*, **4**, 51 (2018).
- I. Buchmann, *Cadex Electron Inc*, 29 (2001).
- J. E. Dutrizac, *Zinc* **85**, 707, (1985).
- R. M. Morrison, *Hydrometallurgy*, **22**, 67 (1989).
- J. Frenay, *Hydrometallurgy*, **15**, 243 (1985).
- V. Stanković, I. Duo, C. Comminellis, and F. Zonneville, *J. Appl. Electrochem.*, **37**, 1279 (2007).
- W.-T. Chen, C.-C. Ma, M.-H. Lee, Y.-C. Chu, L.-C. Tsai, and C.-M. Shu, *Appl. Energy*, **100**, 187 (2012).
- P. A. Ramirez, V. E. Reyes, and M. A. Veloz, *Int J Electrochem Sci*, **6**, 14 (2011).
- V. Tricoli, N. Vatisstas, and P. F. Marconi, *J. Appl. Electrochem.*, **23**, 390 (1993).
- A. V. Pethkar and K. M. Paknikar, *Process Biochem.*, **38**, 855 (2003).
- V. Reyes Cruz, M. T. Oropeza, I. González, and C. Ponce-De-León, *J. Appl. Electrochem.*, **32**, 473 (2002).
- Y. Su, Q. Li, Y. Wang, H. Wang, J. Huang, and X. Yang, *J. Hazard. Mater.*, **170**, 1164 (2009).
- S. Pavlinić and I. Piljac, *Water Res.*, **32**, 2913 (1998).
- H. Koseoglu and M. Kitis, *Miner. Eng.*, **22**, 440 (2009).
- K. G. Adami, R. W. Barley, and R. D. Pascoe, *Miner. Eng.*, **18**, 1269 (2005).
- V. Stanković, L. Outarra, F. Zonneville, and C. Comminellis, *Sep. Purif. Technol.*, **61**, 366 (2008).
- M. S. Alam, K. Inoue, K. Yoshizuka, Y. Dong, and P. Zhang, *Hydrometallurgy*, **44**, 245 (1997).
- K. C. Sole, T. L. Ferguson, and J. B. Hiskey, *Solvent Extr. Ion Exch.*, **12**, 1033 (1994).
- D. Robinson and F. C. Walsh, *J. Photogr. Sci.*, **42**, 182 (1994).
- M. Chatelut, E. Gobert, and O. Vittori, *Hydrometallurgy*, **54**, 79 (2000).
- A. R. Alonso, G. T. Lapidus, and I. González, *Hydrometallurgy*, **92**, 115 (2008).
- R. E. Rettew, J. W. Guthrie, and F. M. Alamgir, *J. Electrochem. Soc.*, **156**, D513 (2009).
- M. Fayette, Y. Liu, D. Bertrand, J. Nutariya, N. Vasiljevic, and N. Dimitrov, *Langmuir*, **27**, 5650 (2011).
- N. Jayaraju, D. Vairavapandian, Y. G. Kim, D. Banga, and J. L. Stickney, *J. Electrochem. Soc.*, **159**, D616 (2012).
- Y. Yu, Y. Hu, X. Liu, W. Deng, and X. Wang, *Electrochimica Acta*, **54**, 3092 (2009).
- Y.-G. Kim, J. Y. Kim, D. Vairavapandian, and J. L. Stickney, *J. Phys. Chem. B*, **110**, 17998 (2006).
- L. B. Sheridan, J. Czerwiniski, N. Jayaraju, D. K. Gebregziabher, J. L. Stickney, D. B. Robinson, and M. P. Soriaga, *Electrocatalysis*, **3**, 96 (2012).
- S. R. Brankovic, J. X. Wang, and R. R. Adžić, *Surf. Sci.*, **474**, L173 (2001).
- L. C. Grabow, Q. Yuan, H. A. Doan, and S. R. Brankovic, *Surf. Sci.*, **640**, 50 (2015).
- T. S. Mkwizu, M. K. Mathe, and I. Cukrowski, *J. Electrochem. Soc.*, **160**, H529 (2013).
- K. Yliniemi, D. Wragg, B. P. Wilson, H. N. McMurray, D. A. Worsley, P. Schmuki, and K. Kontturi, *Electrochimica Acta*, **88**, 278 (2013).
- T. S. Mkwizu, M. K. Mathe, and I. Cukrowski, *Langmuir*, **26**, 570 (2010).
- P. Halli, H. Elomaa, B. P. Wilson, K. Yliniemi, and M. Lundström, *ACS Sustain. Chem. Eng.*, **5**, 10996 (2017).
- K. Yliniemi, N. T. Nguyen, S. Mohajernia, N. Liu, B. P. Wilson, P. Schmuki, and M. Lundström, *J. Clean. Prod.*, **201**, 39 (2018).
- I. Korolev, P. Altunkaya, P. Halli, P.-M. Hannula, K. Yliniemi, and M. Lundström, *J. Clean. Prod.*, **186**, 840 (2018).
- K. Yliniemi, Z. Wang, I. Korolev, P. Hannula, P. Halli, and M. Lundström, *ECS Trans.*, **85**, 59 (2018).
- A. E. Saba and A. E. Elsherief, *Hydrometallurgy*, **54**, 91 (2000).
- G. T. Wever, *JOM*, **11**, 130 (1959).
- L. Mureşan, G. Maurin, L. Oniciu, and D. Gaga, *Hydrometallurgy*, **43**, 345 (1996).
- T. Boiadjieva, M. Monev, A. Tomandl, H. Kronberger, and G. Fafilek, *J. Solid State Electrochem.*, **13**, 671 (2009).
- R. C. M. Salles, G. C. G. de Oliveira, S. L. Díaz, O. E. Barcia, and O. R. Mattos, *Electrochimica Acta*, **56**, 7931 (2011).
- J. O. Bockris and E. C. Potter, *J. Electrochem. Soc.*, **99**, 169 (1952).
- M. G. Chu, J. McBreen, and G. Adzic, *J. Electrochem. Soc.*, **128**, 2281 (1981).
- A. R. Despić and M. G. Pavlović, *Electrochimica Acta*, **27**, 1539 (1982).
- G. Adzic, J. McBreen, and M. G. Chu, *J. Electrochem. Soc.*, **128**, 1691 (1981).
- C. C. Ho, K. Murata, D. A. Steingart, J. W. Evans, and P. K. Wright, *J. Micromechanics Microengineering*, **19**, 094013 (2009).
- W. M. Haynes, *CRC Handbook of Chemistry and Physics*, 93rd Edition, p. 2657, CRC Press, (2012).
- M. Sánchez Cruz, F. Alonso, and J. M. Palacios, *J. Appl. Electrochem.*, **23**, 364 (1993).
- J.-W. Kim, J.-Y. Lee, and S.-M. Park, *Langmuir*, **20**, 459 (2004).
- H. Van Parys, G. Teliás, V. Nedashkivskiy, B. Mollay, I. Vandendael, S. Van Damme, J. Deconinck, and A. Hubin, *Electrochimica Acta*, **55**, 5709 (2010).
- B. Scharifker and G. Hills, *Electrochimica Acta*, **28**, 879 (1983).